Available online at www.sciencedirect.com
ScienceDirect
Composite Structures 88 (2009) 65–82
COMPOSITE STRUCTURES
www.elsevier.com/locate/compstruct

A strain-rate dependent micro-mechanical model with progressive post-failure behavior for predicting impact response of unidirectional composite laminates

Ala Tabiei *, S. Babu Aminjikarai

Department of Aerospace Engineering and Engineering Mechanics, University of Cincinnati, OH 45221, USA

Available online 23 February 2008

Abstract

A new micro-mechanical model is developed to predict the behavior of unidirectional polymer matrix composite laminates under impact loading conditions and implemented in the non-linear finite element software LS-DYNA. This model accounts for the progressive post-failure behavior and strain-rate dependency of polymer matrix composites making it suitable for impact simulations. A continuum damage mechanics (CDM) based failure model is used to incorporate the progressive post-failure behavior. A set of Weibull distribution functions are used to quantify damage evolution and corresponding reduction in stiffness in different modes in the fibers. Similar functions based on strains are used for the resin. Fiber breakage is assumed as the only ultimate failure mode. In addition to these micro-failure modes, delamination, which is a macro-level failure, is also incorporated using an approach developed earlier for a ply-level progressive failure model. Strain-rate dependent behavior is incorporated by assuming viscoplastic constitutive relations for the resin. Additionally, the in-plane shear modulus of the fiber is also assumed to be rate dependent. Experimental results available in the literature are used to validate the model's predictions.

Keywords: Polymer matrix composites; Unidirectional composites; Micro-mechanical model; Impact response; Continuum damage mechanics; Delamination

1. Introduction

Composite materials are used as structural members in a wide range of applications involving impact such as crashworthiness, protective armors in air and space vehicles. Studies on the response of composites to impact loading have shown that such loading can cause a substantial amount of damage resulting in significant reductions in their strength and stiffness. Also, various modes of damage such as fiber breakage, matrix cracking, and delamination are found to occur in varying proportions depending on parameters such as the projectile mass, velocity, kinetic energy, shape of the end of the projectile, the span of the target, and boundary conditions [1]. It is a widely accepted fact that it is difficult to predict the exact mode and extent of such damages, thereby making this behavior one of the most important aspects that inhibits widespread application of composite materials. This has naturally resulted in extensive studies in this field in recent years. A large number of reports on impact damage in composite structures are available in the literature [1–7] detailing experimental investigations, and analytical and numerical models that have been developed. But there exists no universal approach for the prediction or the representation of the behavior of composite structures under impact loading [2].

Due to the sophisticated computing technology available now, finite element (FE) simulations have become a widely used approach for studying the damage development in composites. New material models are developed and implemented in FE software to provide detailed

* Corresponding author.
E-mail address: ala.tabiei@uc.edu (A. Tabiei).

0263-8223/$ - see front matter © 2008 Elsevier Ltd. All rights reserved.
doi:10.1016/j.compstruct.2008.02.017

information on the spatial and temporal distribution of damage during impact [7]. The transient non-linear FE code LS-DYNA [8] is a popular and powerful software for such efforts as it offers users a very simple interface to implement their own material models.

Current composite models in LS-DYNA are all macro-mechanical models which require the effective properties of composites as input. These models assume that the response of an individual lamina is linear elastic (or non-linear elastic in in-plane shear) up to failure. The various models differ, however, in their formulation of failure criteria used to signal the onset of damage in a lamina [7]. They use different failure criteria to predict different fiber and matrix modes and model failure by reducing dominant stiffness and stress components instantaneously to zero. Physically, this type of modeling is equivalent to assuming ideally brittle post-failure behavior and has been shown to be unrealistic. In addition to the in-built models in LS-DYNA, there are also two additional models, MAT 161 and 162, for unidirectional and fabric composites, respectively, which have been developed and implemented by Materials Sciences Corporation. These models use the continuum damage mechanics (CDM) approach for failure and have been shown to be effective in modeling composite behavior under high strain rate conditions. Recent research suggests that the damage growth in the vicinity of a crack tip or fracture site in a polymeric composite structure manifests itself in the form of strain softening of the material. Strain-softening behavior can be more rigorously dealt with through models based on CDM [7]. Matzenmiller et al. [9] developed a rigorous composite damage model, based on the principles of CDM for the non-linear analysis of composite materials. Later studies by Williams and Vaziri [7] and Van Hoof et al. [10] have shown that such progressive post-failure models based on CDM improve the prediction of impact damage of composite structures significantly. A brief discussion of the origin, development, and broad spectrum of applications of CDM is given in Williams and Vaziri [7].

Another behavior characteristic of polymer matrix composites that is important in impact simulations is their strain-rate dependency. A review of the literature on this topic is given in Goldberg [11]. Most of the three-dimensional materials presented in the literature for rate sensitivity of composites are empirical and consider the entire lamina to be rate-sensitive [11]. Since some fibers are rate-sensitive and some are not while almost all matrix materials are rate-sensitive, care must be taken to separate the effect of the constituents on the composite. For this purpose, micro-mechanics equations, in which the effective behavior of the composite is computed based on the properties and response of the individual constituents, are most suitable for this application [12].

The objective of the present work is to develop a three-dimensional material model to predict the response of unidirectional composites under impact loading conditions and implement it in LS-DYNA. As explained in the following sections, this is achieved by using: (1) micro-mechanics and iso-strain assumptions to develop the equations relating stresses and strains of constituents to the average lamina values; (2) a CDM based approach to model the progressive post-failure behavior; and (3) viscoplastic constitutive relations for the resin to model strain-rate sensitivity.

2. Micro-mechanical model

The representative volume cell (RVC) used to develop the micro-mechanical relations is shown in Fig. 1. This RVC was originally proposed by Pecknold and Rahman [13] and has been used later by Tabiei and Chen [14] and Tabiei et al. [12]. The fibers are assumed to be of square cross-section for computational efficiency since this model is implemented in an explicit FE code which uses very small time steps for simulations. The unit cell is divided into three sub-cells: one fiber sub-cell, denoted as ***f***, and two matrix sub-cells, denoted as $\boldsymbol{M_A}$ and $\boldsymbol{M_B}$, respectively. The three sub-cells are grouped into two parts: material part ***A*** consists of the fiber sub-cell ***f*** and the matrix sub-cell $\boldsymbol{M_A}$, and material part ***B*** consists of the remaining matrix $\boldsymbol{M_B}$. The dimensions of the unit cell are 1×1 unit square. The dimensions of the fiber and matrix sub-cells are denoted by W_f and W_m, respectively, as shown in Fig. 1 and defined as below (see [13])

$$W_\mathrm{f} = \sqrt{V_\mathrm{f}}, \quad W_\mathrm{m} = 1 - W_\mathrm{f} \tag{1}$$

where V_f is the fiber volume fraction [13]. As explained in a later section, effective stresses in the RVC are determined from the sub-cell values in two phases: first, stresses in fiber ***f*** and matrix $\boldsymbol{M_A}$ are combined to obtain effective stresses in part ***A*** which are then combined with stresses in matrix $\boldsymbol{M_B}$ to obtain the effective RVC stresses.

The following assumptions are made regarding behavior of the constituents and the composite as a whole.

1. The matrix constituent i.e. resin is a homogeneous, viscoplastic material that is initially isotropic but becomes orthotropic with damage evolution, if any.

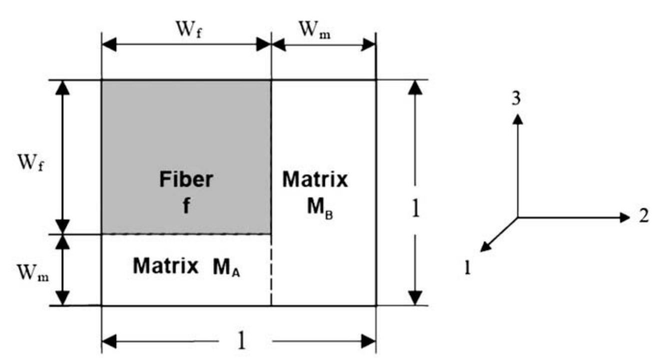

Fig. 1. Representative volume cell (RVC) of unidirectional fiber reinforced polymer composites used to develop the micro-mechanical model.

2. The reinforcing constituent i.e. fibers is a homogeneous, linearly elastic material that is initially transversely isotropic but becomes orthotropic with damage evolution, if any.
3. The fibers govern the behavior of the composite in direct loading and the resin in shear. As a consequence of this assumption, only damages to fibers that affect direct stresses and damages to resin that affect shear stresses are taken into account.
4. The fibers are positioned in the matrix such that the composite lamina is a homogeneous material on the macro-mechanical scale.
5. There is a complete and strong bond at the interface of the constituent materials.

As mentioned above, the matrix material is assumed to be a viscoplastic material. When plasticity is involved in a micro-mechanical model, the iso-stress boundary conditions between some constituents cause big difficulty. The plastic strain is an additional redundant unknown and the boundary conditions are not enough to solve the problem for all of the unknowns. The iso-strain boundary conditions are widely used in the micro-mechanical approach of composite materials although for elastic property prediction it is known that they do not give the best result. Iso-strain boundary conditions are assumed for all the three sub-cells of the RVC in order to avoid any difficulties and to simplify the calculations. This means that the strain tensor as well as the tensor of the strain-rate is the same for all points of the RVC [15].

The material model is implemented for solid (brick) elements in LS-DYNA. The strain-rate is received as input by the material model and the stresses are computed and returned as output. So, the objective of material model development is to determine the stress response of the RVC for a given strain-rate at each time step. As described in the following sections, the stresses in the RVC are determined from the stresses in the constituents (sub-cells) which are in-turn determined from their individual properties and the total strains. Hence, the total strains of the RVC are accumulated from the strain-rates at each time step using the following relation and stored as history variables.

$$\varepsilon_{ij}^{(n+1)} = \varepsilon_{ij}^{(n)} + \dot{\varepsilon}_{ij}^{(n)}\mathrm{d}t, \quad i,j = 1,2,3 \tag{2}$$

3. Viscoplastic constitutive relations for matrix material

Polymer matrix composites exhibit strain-rate dependent deformation behavior, especially for the matrix dominated properties. Experimental studies have shown that this behavior is primarily due to the viscoplastic nature of resins that are used as matrix materials. Hence, strain-rate dependency is incorporated in the current model by assuming a viscoplastic relationship developed by Goldberg and Stouffer [16] for the matrix constituent (sub-cells $\mathbf{M}_A$ and $\mathbf{M}_B$). They developed this constitutive relationship for resins using the state variable approach and used it in their material model for unidirectional composites. They defined their state variable as an internal stress, which evolved with stress and inelastic strain and represented the average effects of the deformation mechanisms. This approach has also been used in other similar works [12,15,17] to model polymer matrix composites and shown to be effective. For completeness, the Goldberg–Stouffer relations are discussed briefly in this section. Further details about the relations can be found in [16].

The total strain-rate is assumed to be the sum of elastic and inelastic strain-rates. The elastic strain-rate is equal to the ratio of stress rate to Young's modulus of the material while the inelastic strain-rate is defined to be proportional to the exponential of the overstress, the difference between the applied stress and the tensorial internal stress state variable. It is given by the relation:

$$\dot{\varepsilon}_{ij}^{I} = D_0 \exp\left[-\frac{1}{2}\left(\frac{Z_0^2}{3K_2}\right)^{n}\right]\frac{S_{ij} - \Omega_{ij}}{\sqrt{K_2}} \tag{3}$$

where $\dot{\varepsilon}_{ij}^{I}, \Omega_{ij}$ are the components of inelastic strain-rate, and internal stress, respectively, D_o is a scale factor representing maximum inelastic strain-rate, n is a variable which controls rate dependence of the deformation response, Z_o represents the isotropic, initial hardness of the material before any load is applied, S_{ij} are components of the deviatoric stress tensor given by the relation:

$$S_{ij} = \frac{\sigma_{ij} - \delta_{ij}\sigma_{kk}}{3} \tag{4}$$

where σ_{ij} are the components of stress, and δ_{ij} is Kronecker's delta. K_2 in Eq. (3) is defined as an effective stress given by the relation:

$$K_2 = \frac{1}{2}(S_{ij} - \Omega_{ij})(S_{ij} - \Omega_{ij}) \tag{5}$$

and represents the second variant of the overstress tensor. D_o, Z_o and n are material constants which are determined from experiments. The procedure for determining them can be found in [16].

The internal stress rate is given by the relation:

$$\dot{\Omega}_{ij} = \frac{2}{3}q\Omega_{\mathrm{m}}\dot{\varepsilon}_{ij}^{I} - q\Omega_{ij}\dot{\varepsilon}_{e}^{I} \tag{6}$$

where Ω_{ij}, $\dot{\Omega}_{ij}$ and $\dot{\varepsilon}_{ij}^{I}$ are components of internal stress, internal stress rate, and inelastic strain-rate, respectively, and $\dot{\varepsilon}_{e}^{I}$ is effective inelastic strain-rate given by the relation:

$$\dot{\varepsilon}_{e}^{I} = \sqrt{\frac{2}{3}\dot{\varepsilon}_{ij}^{I}\dot{\varepsilon}_{ij}^{I}} \tag{7}$$

It is to be noted that Eqs. (3)–(7) actually formulate one differential equation per component of the tensorial parameters involved or one first order tensorial differential equation which has no closed form solution. Hence, a numerical solution is obtained at each time step of the explicit FE simulation.

The explicit time integration method requires small time steps for a stable solution and it is provided in such a FE code, but still in impact situations a high strain increment could appear despite the small time step. In order to ensure stability of the differential equation solution, the four-step Runge–Kutta method is adopted here [15]. Eqs. (3), (6), and (7) are converted to their incremental forms for this purpose and implemented in the model. Incremental forms of the equations are obtained by multiplying the rate equations by the time step dt. The resulting equations are as follows:

$$\mathrm{d}\varepsilon_{ij}^{I} = \left(D_0 \exp\left[-\frac{1}{2}\left(\frac{Z_0^2}{3K_2}\right)^n \right] \frac{S_{ij} - \Omega_{ij}}{\sqrt{K_2}} \right) \mathrm{d}t \tag{8}$$

$$\mathrm{d}\Omega_{ij} = \left(\frac{2}{3} q \Omega_{\mathrm{m}}\, \mathrm{d}\varepsilon_{ij}^{I} - q \Omega_{ij}\, \mathrm{d}\varepsilon_{e}^{I} \right) \mathrm{d}t \tag{9}$$

$$\mathrm{d}\varepsilon_{e}^{I} = \left(\sqrt{\frac{2}{3}\mathrm{d}\varepsilon_{ij}^{I}\,\mathrm{d}\varepsilon_{ij}^{I}} \right) \mathrm{d}t \tag{10}$$

where the terms are as defined earlier but some with prefix d representing their incremental values.

At time step $n+1$ of the explicit time integration, the following values are available and are all used as input parameters for the matrix material stress response calculation: stress of the matrix material from the previous time step $n, \sigma_{ij}^{\mathrm{m}(n)}$, strain at the current time step, $\varepsilon_{ij}^{(n+1)}$, strain-rate at the current time step, $\dot{\varepsilon}_{ij}^{(n+1)}$, inelastic strain from the previous time step, $\varepsilon_{ij}^{I(n)}$, and the state variable, $\Omega_{ij}^{\mathrm{m}(n)}$. At the first step of the Runge–Kutta method, assume that:

$$\sigma_{ij} = \sigma_{ij}^{\mathrm{m}(n)}, \quad \Omega_{ij} = \Omega_{ij}^{\mathrm{m}(n)} \tag{11}$$

Then, applying Eqs. (3)–(10), the results for inelastic strain increment and for state variable increment are denoted as follows:

$$\mathrm{d}\varepsilon_{ij}^{I1} = \mathrm{d}\varepsilon_{ij}^{I}, \quad \mathrm{d}\Omega_{ij}^{1} = \mathrm{d}\Omega_{ij} \tag{12}$$

Then, the inelastic strain, stress, and state variable are updated as follows:

$$\varepsilon_{ij}^{I} = \varepsilon_{ij}^{I(n)} + \frac{1}{2}\mathrm{d}\varepsilon_{ij}^{I1} \tag{13}$$

$$\{\sigma\} = [C_{\mathrm{m}}](\{\varepsilon\}^{(n+1)} - \{\varepsilon^{I}\}) \tag{14}$$

$$\Omega_{ij} = \Omega_{ij}^{\mathrm{m}(n)} + \frac{1}{2}\mathrm{d}\Omega_{ij}^{1} \tag{15}$$

where $[C_{\mathrm{m}}] = \begin{bmatrix} C_{11}^{\mathrm{m}} & C_{12}^{\mathrm{m}} & C_{12}^{\mathrm{m}} & 0 & 0 & 0 \\ & C_{11}^{\mathrm{m}} & C_{12}^{\mathrm{m}} & 0 & 0 & 0 \\ & & C_{11}^{\mathrm{m}} & 0 & 0 & 0 \\ & & & C_{44}^{\mathrm{m}} & 0 & 0 \\ & \text{Symm.} & & & C_{44}^{\mathrm{m}} & 0 \\ & & & & & C_{44}^{\mathrm{m}} \end{bmatrix}$ is the stiffness matrix of the resin, $C_{11}^{\mathrm{m}} = \frac{E_{\mathrm{m}}(1-\nu_{\mathrm{m}})}{(1+\nu_{\mathrm{m}})(1-2\nu_{\mathrm{m}})}, C_{12}^{\mathrm{m}} = \frac{E_{\mathrm{m}}\nu_{\mathrm{m}}}{(1+\nu_{\mathrm{m}})(1-2\nu_{\mathrm{m}})}, C_{44}^{\mathrm{m}} = G_{\mathrm{m}} = \frac{E_{\mathrm{m}}}{2(1+\nu_{\mathrm{m}})}$, E_{m} is its Young's modulus, ν_{m} is its Poisson's ratio, and G_{m} is its shear modulus.

At the second step, σ_{ij} from Eq. (14) and Ω_{ij} from Eq. (15) are accepted as input parameters and the results of application of Eqs. (3)–(10) are denoted as

$$\mathrm{d}\varepsilon_{ij}^{I2} = \mathrm{d}\varepsilon_{ij}^{I}, \quad \mathrm{d}\Omega_{ij}^{2} = \mathrm{d}\Omega_{ij} \tag{16}$$

Again, the inelastic strain, stress, and state variable are updated as follows:

$$\varepsilon_{ij}^{I} = \varepsilon_{ij}^{I(n)} + \frac{1}{2}\mathrm{d}\varepsilon_{ij}^{I2} \tag{17}$$

$$\{\sigma\} = [C_{\mathrm{m}}](\{\varepsilon\}^{(n+1)} - \{\varepsilon^{I}\}) \tag{18}$$

$$\Omega_{ij} = \Omega_{ij}^{\mathrm{m}(n)} + \frac{1}{2}\mathrm{d}\Omega_{ij}^{2} \tag{19}$$

The input parameters of the algorithm at the third step are σ_{ij} from Eq. (18) and Ω_{ij} from Eq. (19) and the results obtained are:

$$\mathrm{d}\varepsilon_{ij}^{I3} = \mathrm{d}\varepsilon_{ij}^{I}, \quad \mathrm{d}\Omega_{ij}^{3} = \mathrm{d}\Omega_{ij} \tag{20}$$

Before the last step of the Runge–Kutta method (4), the total inelastic strain, stress, and state variable are again updated as follows:

$$\varepsilon_{ij}^{I} = \varepsilon_{ij}^{I(n)} + \mathrm{d}\varepsilon_{ij}^{I3} \tag{21}$$

$$\{\sigma\} = [C_{\mathrm{m}}](\{\varepsilon\}^{(n+1)} - \{\varepsilon^{I}\}) \tag{22}$$

$$\Omega_{ij} = \Omega_{ij}^{\mathrm{m}(n)} + \mathrm{d}\Omega_{ij}^{3} \tag{23}$$

At the fourth and final step, σ_{ij} from Eq. (22) and Ω_{ij} from Eq. (23) are accepted as input parameters and the results of application of Eqs. (3)–(10) are denoted as

$$\mathrm{d}\varepsilon_{ij}^{I4} = \mathrm{d}\varepsilon_{ij}^{I}, \quad \mathrm{d}\Omega_{ij}^{4} = \mathrm{d}\Omega_{ij} \tag{24}$$

Finally, the inelastic strain, stress, and internal state variable of the matrix material can be updated for time step $n+1$ from the previous time step values and the results of the Runge–Kutta steps as follows:

$$\varepsilon_{ij}^{I(n+1)} = \varepsilon_{ij}^{I(n)} + \frac{1}{6}\mathrm{d}\varepsilon_{ij}^{I1} + \frac{1}{3}\mathrm{d}\varepsilon_{ij}^{I2} + \frac{1}{3}\mathrm{d}\varepsilon_{ij}^{I3} + \frac{1}{6}\mathrm{d}\varepsilon_{ij}^{I4} \tag{25}$$

$$\{\sigma\}^{\mathrm{m}(n+1)} = [C_{\mathrm{m}}](\{\varepsilon\}^{(n+1)} - \{\varepsilon^{I}\}^{(n+1)}) \tag{26}$$

$$\Omega_{ij}^{\mathrm{m}(n+1)} = \Omega_{ij}^{\mathrm{m}(n)} + \frac{1}{6}\mathrm{d}\Omega_{ij}^{I} + \frac{1}{3}\mathrm{d}\Omega_{ij}^{II} + \frac{1}{3}\mathrm{d}\Omega_{ij}^{III} + \frac{1}{6}\mathrm{d}\Omega_{ij}^{IV} \tag{27}$$

4. Constitutive relations for fibers

The fibers are assumed to be linearly elastic materials which are initially transversely isotropic but become orthotropic with damage evolution, if any. It is assumed that damages to the fibers are a result of direct stresses applied on them only and that shear stresses do not cause any damages. This corresponds to the assumption that the fiber material properties govern the behavior of unidirectional composites under direct loading and the matrix material properties govern the behavior of composites under shear. The damages are assumed to be oriented in the material directions of the fibers and independent. Finally, it is assumed that damage evolution in the fiber direction leads to ultimate failure of the composite material and there is no other ultimate failure or other damage that contributes to the ultimate failure. The independence of the damages avoids the seeking for a damage dissipation function often utilized in the continuum damage mechanics.

The constitutive relations of the fibers can be written in matrix form as

$$\{\sigma\}^{\mathrm{f}} = [C_{\mathrm{f}}]\{\varepsilon\}^{\mathrm{f}} \tag{28}$$

where $[C_{\mathrm{f}}]$ is their stiffness matrix which can be partitioned into direct and shear stress stiffness matrices as follows:

$$[C_{\mathrm{f}}] = [S_{\mathrm{f}}]^{-1} = \begin{bmatrix} [S_{\mathrm{f}d}]^{-1} & [0]_{3\times 3} \\ [0]_{3\times 3} & [S_{\mathrm{f}s}]^{-1} \end{bmatrix} \tag{29}$$

The direct stress compliance matrix, whose inverse is the direct stress stiffness matrix, should be symmetric and the following relationship should be obeyed:

$$\frac{v_{ij}}{E_i} = \frac{v_{ji}}{E_j} \quad i,j = 1,2,3 \text{ and } i \neq j (\text{no summation}) \tag{30}$$

The direct and shear stress compliance matrices in terms of the properties of the fibers are:

$$[S_{\mathrm{f}d}] = \begin{bmatrix} \frac{1}{(1-d_1)E_1} & -\sqrt{\frac{v_{12}}{(1-d_1)E_1}\frac{v_{21}}{(1-d_2)E_2}} & -\sqrt{\frac{v_{12}}{(1-d_1)E_1}\frac{v_{21}}{(1-d_3)E_2}} \\ & \frac{1}{(1-d_2)E_2} & -\frac{v_{23}}{\sqrt{(1-d_2)E_2(1-d_3)E_2}} \\ \text{Symm.} & & \frac{1}{(1-d_3)E_2} \end{bmatrix} \tag{31}$$

$$[S_{\mathrm{f}s}] = \begin{bmatrix} \frac{1}{G_{12}} & 0 & 0 \\ & \frac{1}{G_{23}} & 0 \\ \text{Symm.} & & \frac{1}{G_{o12}} \end{bmatrix} \tag{32}$$

where E_1, E_2 are the longitudinal and transverse moduli of the fibers, respectively, v_{ij}, i, $j = 1$, 2, 3 and $i \neq j$, are its Poisson's ratios, G_{o12}, G_{12} are its initial and strain-rate dependent in-plane shear moduli respectively, G_{23} is its transverse shear moduli, and d_i, $i = 1$, 2, 3, are damage parameters given in the following section on progressive failure modeling. Strain-rate dependency of the model is confined to the parameters determining the main behavior of unidirectional composites. Since in-plane shear is one of them, the shear modulus G_{12} is defined as strain-rate dependent with the following relationship of dependency:

$$G_{12} = a_G s_{\mathrm{s}} + G_{o12} \tag{33}$$

$$s_{\mathrm{s}} = \frac{1}{t}\int_0^t \log\left(\frac{|\dot{\varepsilon}_{12}|}{\dot{\varepsilon}_o}\right)\mathrm{d}t \tag{34}$$

where a_G is a parameter which expresses the strain-rate sensitivity of G_{12}, t is the time elapsed, G_{o12} is the initial in-plane shear modulus of the fibers, $\dot{\varepsilon}_{12}$ is the in-plane shear strain-rate, $\dot{\varepsilon}_o$ is a basic strain-rate with which the current strain-rates are compared and is accepted as the strain-rate of the static loading for a given working strain-rate range. A time integration of the strain-rates is needed as they are not constant during impact simulations and also because the stress–strain relationship for the fibers is based on their secant stiffness and not tangential stiffness.

5. Progressive failure model

5.1. Damage evolution in constituents

In the current model, damage growth is based on a Weibull distribution of strengths which is commonly associated with the strength of fibers. The Weibull distribution function is chosen as it describes the failure of a bundle of fibers with initial defects very well and reasonably [15].

Following the concept of damage unrecovery, the evolution function for damage describing fiber breakage at time step $n+1$, is expressed as follows:

$$d_1^{(n+1)} = \min\left\{1 - \exp\left[-\frac{1}{m_{\mathrm{f}1}e}\left(\frac{E_1\|\varepsilon_{11}|}{\sigma_{1\mathrm{t|c}}}\right)^{m_{\mathrm{f}1}}\right], d_1^{(n)}\right\} \tag{35}$$

where t|c denotes tension or compression. When $\varepsilon_{11} > 0$, the parameters for tension are utilized and the parameters for compression otherwise. When the damage d_1 reaches 0.99 in tension, the finite element is considered totally failed. $\sigma_{1\mathrm{t|c}}$ is not simply the strength of the fibers but is a reduced value given by the relation:

$$\sigma_{1\mathrm{t|c}} = \frac{X_{\mathrm{t|c}}}{b_{\mathrm{t|c}}} \tag{36}$$

where $X_{\mathrm{t|c}}$ is the tensile/compressive strength of the pure fibers, and $b_{\mathrm{t|c}}$ is a reduction factor. The physical justification for using such a factor is the fact that fibers generally display reduced strengths in unidirectional composites as evidenced by the lower strength of the latter compared to the former in uni-axial longitudinal tension. This factor is determined by simulating uni-axial tensile tests on a single element model and matching the ultimate stress to experimentally observed values.

The damage evolution functions in the fiber transverse directions are similar to the longitudinal one. The properties of the fibers in both transverse directions are the same, therefore the evolution functions as well as their parameters are the same, only the history of the loading is different.

$$d_2^{(n+1)} = \min\left\{1 - \exp\left[-\frac{1}{m_{\mathrm{f}2}e}\left(\frac{E_2|\varepsilon_{22}|}{\sigma_{2\mathrm{t|c}}}\right)^{m_{\mathrm{f}2}}\right], d_2^{(n)}\right\} \tag{37}$$

$$d_3^{(n+1)} = \min\left\{1 - \exp\left[-\frac{1}{m_{\mathrm{f}2}e}\left(\frac{E_2|\varepsilon_{33}|}{\sigma_{2\mathrm{t|c}}}\right)^{m_{\mathrm{f}2}}\right], d_3^{(n)}\right\} \tag{38}$$

The damages in transverse directions of the fibers are constrained to not exceed 0.90 to avoid numerical instabilities.

The concept of effective elastic moduli is accepted for the fiber material damages and the damages are applied on the stiffness coefficients as shown in Eq. (31).

Damages are imposed on the matrix material, but they affect only the shear stresses of the resin, which is considered to have the main contribution to the shear stresses of the RVC. The single Weibull distribution function is accepted again as an evolution function of the damages but it involves the ultimate strain for the damage development rather than the ultimate stress. The damage evolution function for in-plane shear is as follows:

$$d_4^{(n+1)} = \min\left\{1 - \exp\left[-\left(\frac{\alpha_s|\varepsilon_{12}|}{\varepsilon_{4m}}\right)^{m_s}\right], d_4^{(n)}\right\} \tag{39}$$

where ε_{4m} is the ultimate shear strain of the matrix material, and α_s is a factor that is used to control the damage initiation strain and the rate of damage evolution.

Similarly, the damage evolution functions for transverse shear failure of the matrix material at time step $n+1$ are calculated as follows:

$$d_5^{(n+1)} = \min\left\{1 - \exp\left[-\left(\frac{\alpha_s|\varepsilon_{23}|}{\varepsilon_{5m}}\right)^{m_s}\right], d_5^{(n)}\right\} \tag{40}$$

$$d_6^{(n+1)} = \min\left\{1 - \exp\left[-\left(\frac{\alpha_s|\varepsilon_{31}|}{\varepsilon_{4m}}\right)^{m_s}\right], d_6^{(n)}\right\} \tag{41}$$

The damages of the matrix material are constrained to not exceed 0.80. These damages are applied on the matrix material shear stresses when the stress response of the sub-cells is calculated. The concept of effective stress is accepted here for the matrix material, rather than the concept of the effective elastic moduli, because the matrix material model is isotropic while the damages in the material are not. The other reason is that the viscoplastic material model calculates the actual stress of the material, not the effective stress of the damaged material [15]. Note that three different damage exponents are used for the constituent level damage evolution functions: (1) m_{f1} for fiber failure in the longitudinal direction (ultimate failure), (2) m_{f2} for fiber transverse failure and (3) m_s for matrix failure in shear.

5.2. Delamination

A composite lamina model based on the 3D stress field has been developed by MSC to enhance the modeling capability of the progressive failure behavior of composite laminates due to transverse impact. It has been implemented into LS-DYNA as MAT 161. This failure model can be used to effectively simulate fiber failure, matrix damage, and delamination behavior under all conditions – opening, closure, and sliding of failure surfaces. Furthermore, this progressive failure approach is advantageous as it enables one to predict delamination when locations of delamination sites cannot be anticipated i.e. locations of potential delamination initiation is calculated without a priori definition of an inter-laminar crack surface [18]. The approach used in this ply-level model to account for delamination failure is adapted in the current micro-mechanical model.

Delamination is considered to be a failure mode which is due to the quadratic interaction between the through-the-thickness stresses of a lamina and is assumed to be mainly a matrix failure. The loading criterion for this failure mode is assumed to have the following form:

$$S^2\left\{\left(\frac{E_3\langle\varepsilon_{33}\rangle}{S_{3t}}\right)^2 + \left(\frac{G_{23}\gamma_{23}}{S_{230}+S_{SR}}\right)^2 + \left(\frac{G_{31}\gamma_{31}}{S_{310}+S_{SR}}\right)^2\right\} - r^2 = 0 \tag{42}$$

where $\langle\rangle$ are Macaulay brackets, E_3 is the normal tensile modulus of the lamina, G_{23} and G_{31} are the transverse shear moduli of the lamina, S_{3t} is the through-the-thickness tensile strength of the lamina, S_{230} and S_{310} are the transverse shear strengths of the lamina for tensile ε_{33}, r is the damage threshold, and S is a scale factor introduced to provide better correlation of delamination area with experiments which can be determined by fitting analytical prediction to experimental data for the delamination area. Under compressive through-the-thickness strain, $\varepsilon_{33} < 0$, the damaged surface (delamination) is considered to be "closed", and the damage strengths are assumed to depend on the compressive normal strain ε_z similar to Coulomb–Mohr theory i.e.

$$S_{SR} = E_3 \tan\varphi\langle-\varepsilon_z\rangle \tag{43}$$

where φ is Coulomb's friction angle. Effective moduli of the lamina used in Eq. (42) are computed at the first time step and stored as material properties.

$d_{lam}^{(n+1)}$ is the damage variable associated with this failure mode and its evolution is given by the relation:

$$d_{lam}^{(n+1)} = \min\left\{1 - \exp\left[\frac{1}{m_d}(1 - r^{m_d})\right], d_{lam}^{n}\right\} \tag{44}$$

where r is the damage threshold as given in Eq. (42) and m_d is the damage exponent for delamination. Delamination damage is constrained to not exceed 0.90 to avoid numerical difficulties and when this minimum value is reached in an element, it is considered to be fully delaminated. Note that the delamination damage exponent is assumed to be different from the constituent level damage evolution functions given earlier.

When delamination failure given by Eq. (42) occurs in an element, it is assumed that there is no in-plane damage within the element and the load carrying behavior in the through-the-thickness direction is assumed to depend on the opening or closing of the damage surface. Similar to the matrix failure modes, the concept of effective stresses is accepted for this failure mode and damages are applied on the effective RVC stresses as defined in the following section using damage variables $d_z^{(n+1)}, d_{yz}^{(n+1)}$, and $d_{zx}^{(n+1)}$ defined as follows:

$$\text{For tensile mode, } \varepsilon_{33} > 0: d_z^{(n+1)}, d_{yz}^{(n+1)}, d_{zx}^{(n+1)} = d_{lam}^{(n+1)} \tag{45}$$

$$\text{For compressive mode, } \varepsilon_{33} < 0: d_{yz}^{(n+1)}, d_{zx}^{(n+1)} = d_{lam}^{(n+1)} \tag{46}$$

For tensile mode, all the through-the-thickness stress components σ_{33}, σ_{23} and σ_{31} of RVC are reduced while for compressive mode, the damage surface is considered to be closed, and thus, σ_{33} is assumed to be elastic and only σ_{23} and σ_{31} are reduced.

6. Stress calculations

The effective stresses in the RVC are determined from the sub-cell values in two phases: first, stresses in the fiber $\boldsymbol{f}$ and matrix $\boldsymbol{M_A}$ are used to determine the effective stresses of part $\boldsymbol{A}$; then these stresses and the stresses in matrix $\boldsymbol{M_B}$ are used to determine the effective stresses in the RVC.

As mentioned earlier, iso-strain boundary conditions are assumed for all the three sub-cells of the RVC. This implies the rule of mixture for the stress calculations. The simple rule of mixture applied on all components of the fiber and the matrix material stresses means physically that the fiber and matrix materials act in parallel in all directions under loading, which is definitely not realistic. However, this assumption is made in order to simplify the micromechanical relations.

The direct stresses of part $\boldsymbol{A}$ are calculated from the direct stresses of the fiber sub-cell $\boldsymbol{f}$ and the matrix sub-cell $\boldsymbol{M_A}$ using the following relations:

$$\sigma_{11}^{A} = W_{\mathrm{f}}\sigma_{11}^{\mathrm{f}} + (1 - W_{\mathrm{f}})\sigma_{11}^{\mathrm{m}_A} \tag{47}$$

$$\sigma_{22}^{A} = W_{\mathrm{f}}\sigma_{22}^{\mathrm{f}} + (1 - W_{\mathrm{f}})\sigma_{22}^{\mathrm{m}_A} \tag{48}$$

$$\sigma_{33}^{A} = W_{\mathrm{f}}\sigma_{33}^{\mathrm{f}} + (1 - W_{\mathrm{f}})\sigma_{33}^{\mathrm{m}_A} \tag{49}$$

The behavior of unidirectional composites under shear is dominated by the behavior of the matrix material. The contribution of the fibers to the shear stress is very low compared to the contribution of the matrix material. Hence, ad hoc volume fraction coefficients are implemented for shear and a rule of mixture involving them is applied. Then, the shear stress of part $\boldsymbol{A}$ is determined, applying the damages of the matrix material introduced in the previous section, as follows:

$$\sigma_{12}^{A} = V_{\mathrm{s4}}\sigma_{12}^{\mathrm{f}} + (1 - V_{\mathrm{s4}})(1 - d_4)\sigma_{12}^{\mathrm{m}_A} \tag{50}$$

$$\sigma_{23}^{A} = V_{\mathrm{s5}}\sigma_{23}^{\mathrm{f}} + (1 - V_{\mathrm{s5}})(1 - d_5)\sigma_{23}^{\mathrm{m}_A} \tag{51}$$

$$\sigma_{31}^{A} = V_{\mathrm{s4}}\sigma_{31}^{\mathrm{f}} + (1 - V_{\mathrm{s4}})(1 - d_6)\sigma_{31}^{\mathrm{m}_A} \tag{52}$$

The shear volume fraction coefficients, V_{s4} and V_{s5}, are different for the in-plane and transverse shear. They have values quite lower than the volume fraction of the fibers. Since the matrix material is modeled as viscoplastic and the fibers are modeled as elastic, after the saturation of the plasticity in the matrix material, the contribution of the fibers to the shear stress of the sub-cells plays a role of strain hardening.

Finally, the effective stresses in the RVC are obtained by applying the rule of mixtures again which yields the following relations including the softening of through-the-thickness components due to delamination failure as follows:

$$\begin{Bmatrix} \sigma_{11} \\ \sigma_{22} \\ \sigma_{33} \\ \sigma_{12} \\ \sigma_{23} \\ \sigma_{31} \end{Bmatrix}_{\mathrm{RVC}} = \begin{bmatrix} 1 & 0 & 0 & 0 & 0 & 0 \\ & 1 & 0 & 0 & 0 & 0 \\ & & d_z^{(n+1)} & 0 & 0 & 0 \\ & & & 1 & 0 & 0 \\ & \text{Symm.} & & & d_{yz}^{(n+1)} & 0 \\ & & & & & d_{zx}^{(n+1)} \end{bmatrix} \times \left(W_{\mathrm{f}} \begin{Bmatrix} \sigma_{11} \\ \sigma_{22} \\ \sigma_{33} \\ \sigma_{12} \\ \sigma_{23} \\ \sigma_{31} \end{Bmatrix}_{A} + W_{\mathrm{m}} \begin{Bmatrix} \sigma_{11} \\ \sigma_{22} \\ \sigma_{33} \\ \sigma_{12} \\ \sigma_{23} \\ \sigma_{31} \end{Bmatrix}_{M_B} \right) \tag{53}$$

The total strains of the RVC, the total stresses in the matrix material, the internal state variables of the matrix material, the damage variables, and the time average strain-rate logarithms, S_{d} and S_{s}, are kept as history variables at each time step of the explicit time integration process for the next time step calculations.

7. Numerical results and discussion

7.1. Impact of CFRP plates made of T800H/3900-2 fiber/resin system

In this verification example, an impact event with a nominal incident energy level of 33.4 *J* imparted on CFRP plates made of T800H/3900-2 fiber/resin system with a laminate stacking sequence of $[45/90/{-45}/0]_{3S}$ and total thickness of 4.65 mm is simulated using the current material model and LS-DYNA. Contact force–time history and the back face fiber damage due to this impact event has been determined by experiments and is available in [7]. These experimental results were originally obtained as part of a series of drop-weight (high mass, low velocity) and gas-gun (low mass, high-velocity) impact tests [19–21] and were used by Williams and Vaziri [7] to evaluate the predictive capability of a plane-stress CDM based model for composite materials that they implemented in LS-DYNA.

Due to the relatively high stiffness of the test apparatus compared to the transverse stiffness of the composite plate, Williams and Vaziri [7] made the following two simplifying assumptions for their FE simulations. First, the plate was considered to be simply supported all around the perimeter of the test frame rectangular opening of size 127 mm × 76.2 mm. Second, the hemispherical steel impactor (25.4 mm in diameter) was treated as rigid and only the contact surface was discretized using rigid shell elements [7]. These assumptions were validated by Williams and Vaziri [7] by comparing results from the simplified model to a more sophisticated model that took into account the flexibility of the impactor and the supporting frame. The same assumptions are made in the FE simulations using the current model also. However, unlike their simulations which used shell elements, the laminate is discretized using solid elements here since the current model is implemented for solid elements. Also, the mid-plane nodes of the laminate are constrained in the Z-direction to duplicate the simply supported boundary condition of the shell elements.

Material properties of the constituents and other parameters involved in the micro-mechanical model are presented in Table 1. All the input values required for the current model are not available in [7]. The unavailable values are either obtained from literature [11,15] or realistic estimates are used. For example, the transverse modulus of T800H fibers is not available in literature. It is assumed to be about 1/15th of its longitudinal modulus which is the typical case with most fibers. Similarly for the toughened 3900-2 Epoxy resin, the parameters required for its viscoplatic constitutive relations are not available directly in literature and neither are their uni-axial and shear responses at different strain-rates from which they can be determined. The values used for 3501-6 Epoxy, which is also a similar toughened Epoxy, in [15] are used as approximate values.

Fig. 2 shows typical tensile stress–strain behaviors predicted by the current model for different values of the damage parameter m_{f1}. It can be clearly seen from the curves that a small value of m_{f1} makes the material behave in a very ductile manner and the behavior becomes increasingly brittle as m_{f1} increases. It is well known that it is difficult to obtain the softening response of most quasi-brittle materials including fiber-reinforced composites. The softening response heavily depends on the setup and test machines, which can lead to very scattered results. Consequently, the choice of damage parameters for each mode becomes an open issue [22]. Another issue that is generally acknowledged in numerical analysis literature is the mesh sensitivity of results obtained using material models similar to the current one. This is usually overcome by performing a convergence study as part of the numerical investigation. Due to these known issues, multiple simulations are performed using different mesh sizes and different values of the damage parameters m_{f1}, m_{f2}, m_s, and m_d to analyze the predictive capability of the current model.

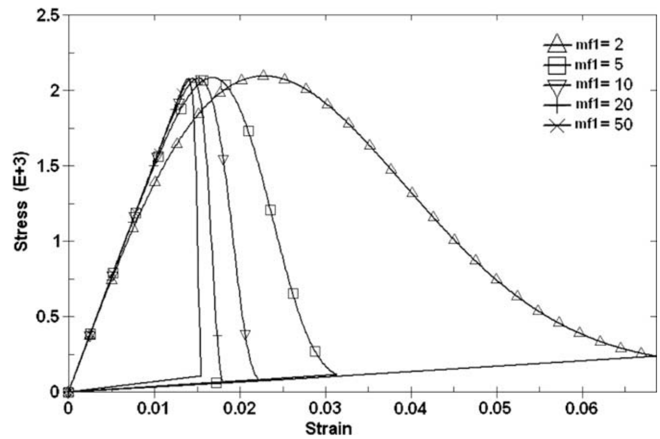

Fig. 2. Longitudinal stress–strain behavior predicted by the current model with different values of damage parameter m_{f1} for a $[45/90/-45/0]_{3S}$ T800H/3900-2 CFRP laminate.

First, the following fixed values are assumed for the material parameters: $S = 1.0; m_{f1} = 20;\ m_{f2} = 20;\ m_s = 6$ and simulations are run using FE models with varying mesh sizes. Delamination failure is de-activated in these cases. Full FE models, similar to the one shown in Fig. 3, with one layer of elements per lamina are used to simulate the impact event. The full laminate, all twenty four plies of it, is modeled using solid elements for all the simulations performed as part of this example since it does not possess any geometric symmetry (due to the presence of +/−45° plies) or periodicity that can be exploited in creating simpler equivalent FE models. The contact force–time history and the back-face fiber damage predicted by the coarsest and the finest FE models are shown in Figs. 4 and 5, respectively, along with the experimental results. As seen in Fig. 4, the contact force history predicted by both these models agrees very well with the experimental result. However, not surprisingly, there is significant difference in the predicted back-face fiber damage with mesh refinement, as seen in Fig. 5. The meshes are successively

Table 1
Properties and parameters of T800H/3900-2 Epoxy and E-glass/Epoxy materials used in verification examples

	V_f (GPa)	$\dot{\varepsilon}_o$ (s^{-1})	E_{o1} (GPa)	ν_{12}	X_t (MPa)	X_c (MPa)	E_2 (GPa)	ν_{23}
T800H/3900-2 Epoxy	0.51	1×10^{-3}	294	0.25	5490	1600	19.6	0.25
E-glass/Epoxy	0.43	1×10^{-4}	74	0.25	3500	1600	4.93	0.25
	σ_{2t} (MPa)	σ_{2c}(MPa)	G_{o12} (GPa)	a_{f4}	G_{23} (GPa)	ε_{4m}	V_{f4}	a_G (GPa)
T800H/3900-2 Epoxy	400	255	20	0.010	7.26	0.14	0.100	0.80
E-glass/Epoxy	80	255	30	0.011	1.97	0.15	0.014	0.90
	V_{f5}	b_t	b_c	ε_{5m}	E_m (GPa)	ν_m	D_o (s^{-1})	Z_o (MPa)
T800H/3900-2 Epoxy	0.200	1.36	1.00	0.14	3.50	0.34	1×10^6	1070
E-glass/Epoxy	0.020	1.00	1.00	0.15	3.00	0.4	1×10^5	240
	n	q	Ω_{max} (MPa)	S_{3t} (MPa)	S_{230} (MPa)	S_{310} (MPa)	ϕ (°)	
T800H/3900-2 Epoxy	0.50	140	114	79	86	64	20	
E-glass/Epoxy	0.90	210	48	100	86	64	20	

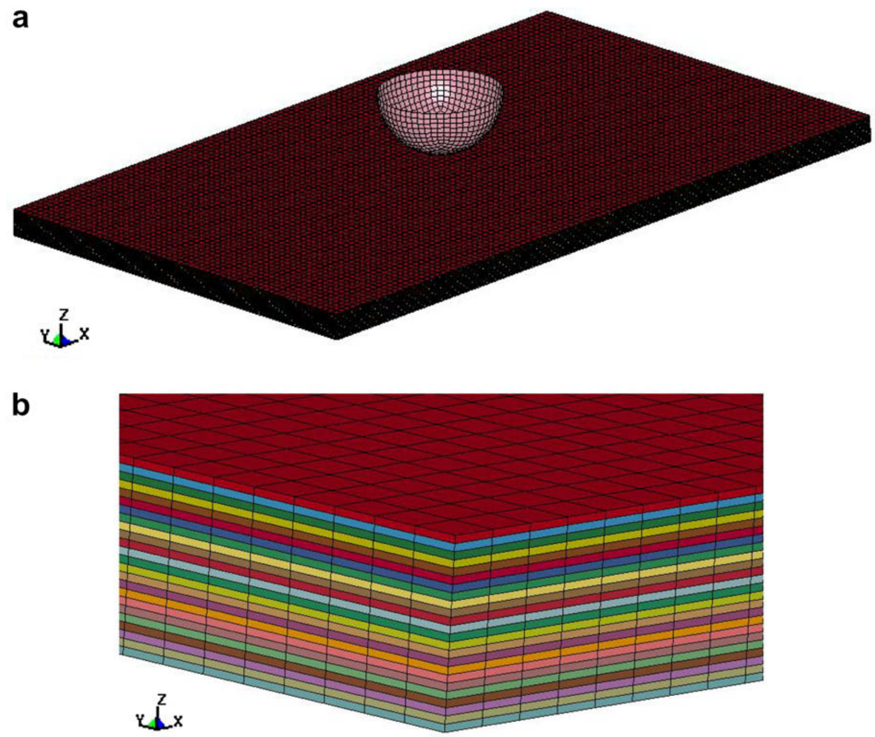

Fig. 3. Example of a FE model used for simulation of a 33.4 *J* impact on a $[45/90/-45/0]_{3S}$ T800H/3900-2 CFRP laminate – (a) full model and (b) close-up view of laminate.

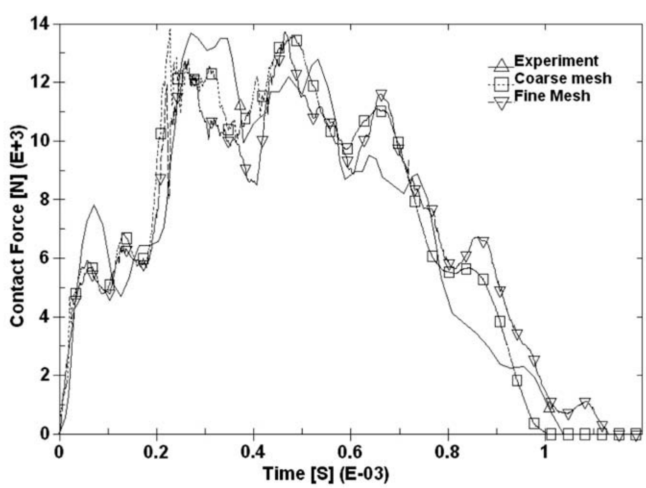

Fig. 4. Contact force–time history predicted by the current model for a 33.4 *J* impact on a $[45/90/-45/0]_{3S}$ T800H/3900-2 CFRP laminate using a coarse mesh and a fine one.

refined until there is no significant difference in the predicted back-face fiber damage.

Next, simulations are run using the finest model for different values of the damage parameters and again the contact force–time history and back-face fiber damage predicted by the model are compared to the experimental result. Figs. 6 and 7 show the results predicted for the following cases along with the experimental result:

(a) $m_{f1} = 2$; *no transverse failure*; *no shear failure*; *no delamination*.
(b) $m_{f1} = 20$; *no transverse failure*; *no shear failure*; *no delamination*.
(c) $m_{f1} = 20$; $m_{f2} = 2$; *no shear failure*; *no delamination*.
(d) $m_{f1} = 20$; $m_{f2} = 20$; *no shear failure*; *no delamination*.
(e) $m_{f1} = 20$; $m_{f2} = 20$; $m_s = 2$ $(\alpha_s = 2.25)$; *no delamination*.
(f) $m_{f1} = 20$; $m_{f2} = 20$; $m_s = 6$ $(\alpha_s = 1.3)$; *no delamination*.
(g) $m_{f1} = 20$; $m_{f2} = 20$; $m_s = 6$ $(\alpha_s = 1.3)$; $m_d = 2$.

In general, the parameter m_{f1} is found to exert the maximum influence on the predicted results. There is a significant drop in the contact force and also a significant increase in the number of failed elements when this parameter is increased from its lowest value (ductile behavior) to its highest value (brittle behavior). Influence of the other parameters is found to be minimal on the predicted contact force. With the various approximations vis-à-vis boundary conditions, approximate values in the constituent properties, reduced integration in the solid elements, etc. made in the simulations, the current model still yields a reasonably accurate contact force–time history. Fig. 7 shows that all the parameters considered exert noticeable influence on the predicted back-face fiber damage. The best result is obtained for *case* (*f*) which is a combination of the highest values of the constituent parameters considered and no delamination. The predicted back-face fiber damage in this case matches closely with the experimental result. When through-the-thickness stiffness reduction due to delamination is also accounted for, the number of failed elements

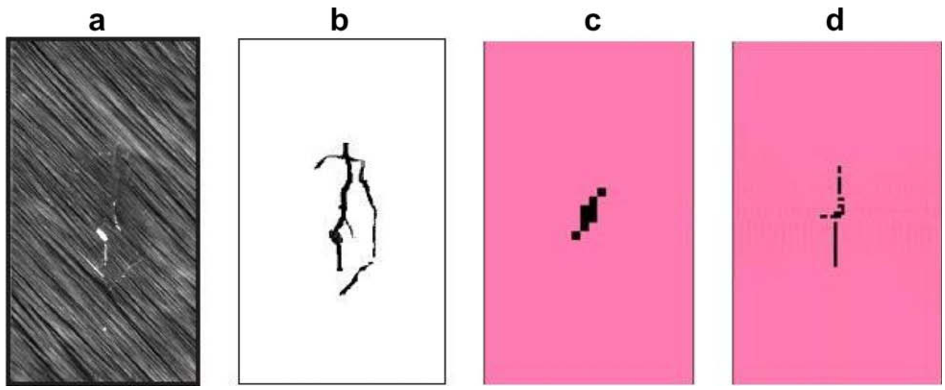

Fig. 5. Back-face fiber damage predicted by the current model for a 33.4 *J* impact on a $[45/90/-45/0]_{3S}$ T800H/3900-2 CFRP laminate: (a and b) experiment (picture taken from Williams and Vaziri [7]), (c) coarse mesh and (d) fine mesh.

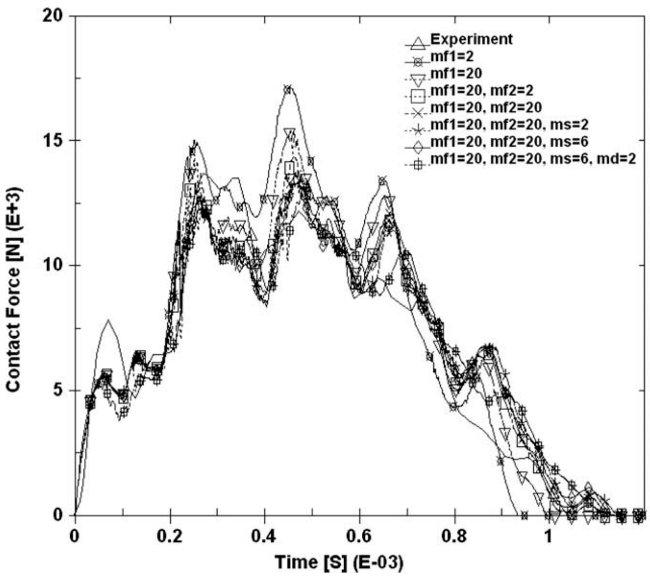

Fig. 6. Contact force–time history predicted by the current model for a 33.4 *J* impact on a $[45/90/-45/0]_{3S}$ T800H/3900-2 CFRP laminate using a fine mesh for different values of the damage parameters.

reduces considerably. These results point to one of the major challenges in developing numerical models for FE simulations of composites with failure. The various failure modes cause a complex re-distribution of stresses which has to be captured reasonably by the models. Aside from this fact, Fig. 7 shows that the current model is capable of closely predicting the back-face fiber damage.

7.2. Impact of 0/90 symmetric E-glass/Epoxy laminate plates

This example involves simulations of impact of 0/90 symmetric E-glass/Epoxy laminated plates with incident energy of 27 *J*. The plates are circular with diameter 200 mm, thickness 1.8 mm, and are made by stacking 10 unidirectional plies with different orientations which are noted $[0_n/90_m/0_n]$, where $2n + m = 10$ with $n = 2,\ 3,\ 4$. Details of the drop-weight set-up and experimental results are given in [1]. The impact is applied at the center of the

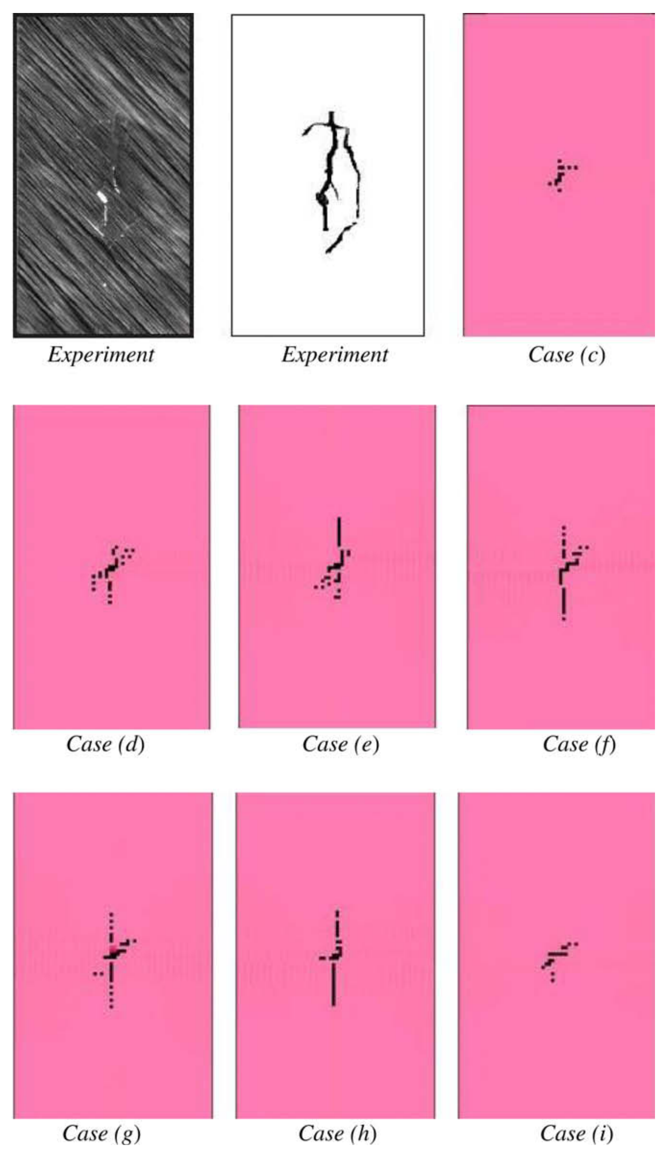

Fig. 7. Back-face fiber damage predicted by the current model for a 33.4 *J* impact on a $[45/90/-45/0]_{3S}$ T800H/3900-2 CFRP laminate using a fine mesh for different values of the damage parameters (pictures of experimental results are taken from Williams and Vaziri [7]).

plate by a cylindrical projectile with a hemispherical end of mass 2.3 kg, density 7.8 kg/m^3, length 600 mm, diameter 25 mm, and having the following properties: $E = 210$ GPa, $\nu = 0.3$. The plates are clamped on their periphery over a 20 mm wide ring and a uniform pressure is applied on the ring by means of springs.

The FE model used for simulations is shown in Fig. 8. As shown in the figure, only a quarter of the experimental set-up is modeled due to symmetry to reduce the computational effort. Each lamina is modeled using a single layer of solid elements. The support is completely constrained at the bottom to make it rigid while the ring is constrained not to move in the vertical Z-direction to account for the pressure applied on it. The latter boundary condition is used since the value of the uniform pressure applied on the springs in the experiments is not given in Ref. [1]. As the following results show, this assumption is found to be sufficient in this case. The impactor is treated as rigid and only the contact surface of the hemispherical end is modeled using shell elements. Eroding surface-to-surface contact is defined between the impactor and the plates and automatic surface-to-surface contact is defined between the support and the plates and also between the ring and the plates. The constituent properties and parameters used in the simulations are given in Table 1. Similar to the previous example, some of the required material properties and parameters which are not available in [1] are either obtained from literature [11,15] or valid estimates are used.

The contact force–time history and the delamination area predicted by the model are compared to experimental results. Since only a quarter model is used in the simulations, the contact force obtained is quadrupled for comparison with the experimental result. Similarly, the delamination area predicted by the model is shown on full plates by reflecting the results about the symmetry planes to make comparisons with the experimental results easier. Mesh sensitivity study is not done but two different meshes are used. First, a sufficiently fine mesh is used to study the variation of predicted results with the damage parameters m_{f2}, m_s, and m_d. Damage parameter m_{f1} is not considered in this study as there is no report of any fiber breakage in the reference paper [1]. Then, based on the observations, a finer mesh is used to check the effect of the scale factor S. Figs. 9–11 show the contact force–time history predicted by the model for different values of the damage parameters considered for the three different configurations. The predicted contact force history is found to be independent of the damage parameters considered for all the three laminates. Contact forces obtained for the $[0_2/90_6/0_2]$ laminate are found to be the closest to its experimental result. Peak force predicted for the $[0_3/90_4/0_3]$ laminate is found to be about 7.1% higher than the experimental value while it is greater by less than 2% for the other two laminates. In all the three laminates, while there is good agreement between the predicted and experimental values in the loading part, the former are relatively much higher in the unloading part suggesting that the model predicts stiffer

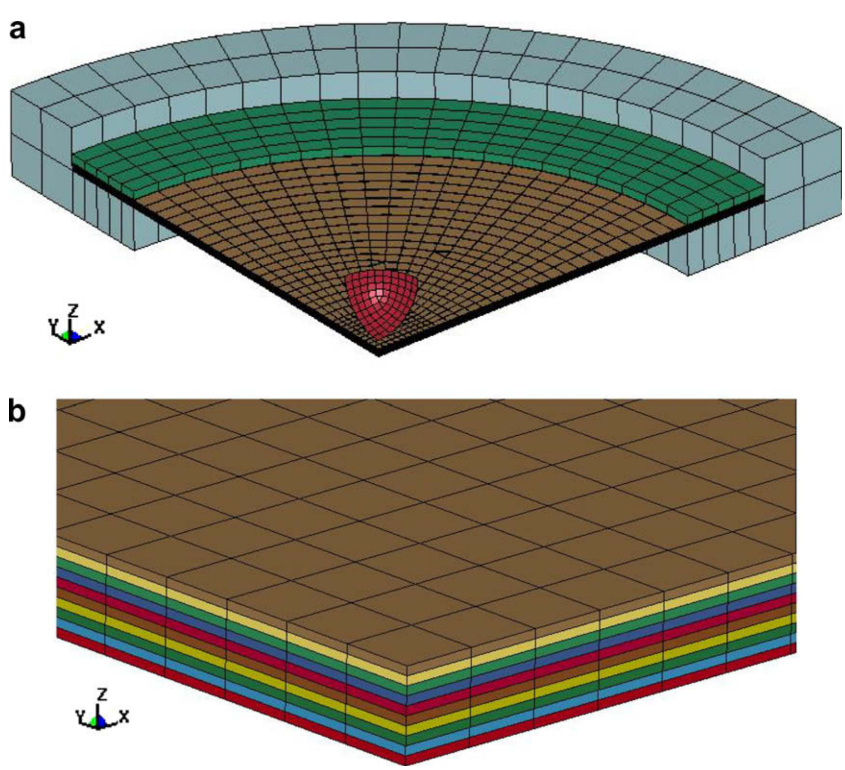

Fig. 8. FE model used for FE simulation of a 27 J impact on $[0_n/90_m/0_n]$, $n = 2, 3, 4$, E-glass/Epoxy laminates – (a) full model and (b) close-up view of laminate.

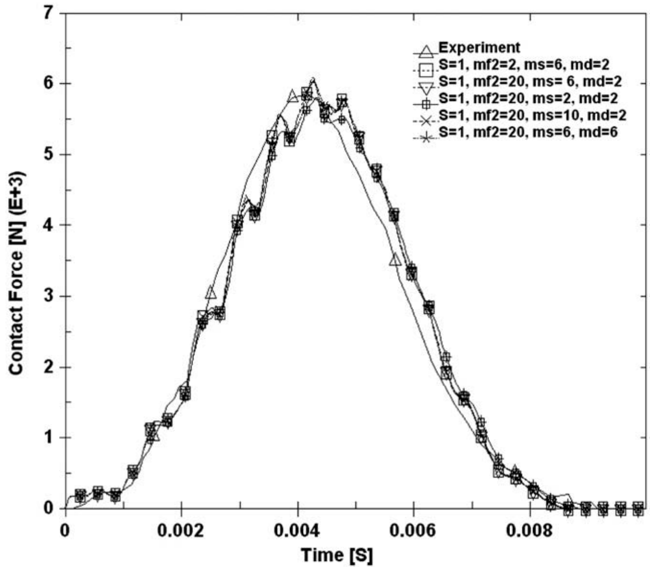

Fig. 9. Contact force–time history predicted by the current model using different values of damage parameters m_{f2},m_s, and m_d for a 27 *J* impact on a $[0_2/90_6/0_2]$ E-glass/Epoxy laminate.

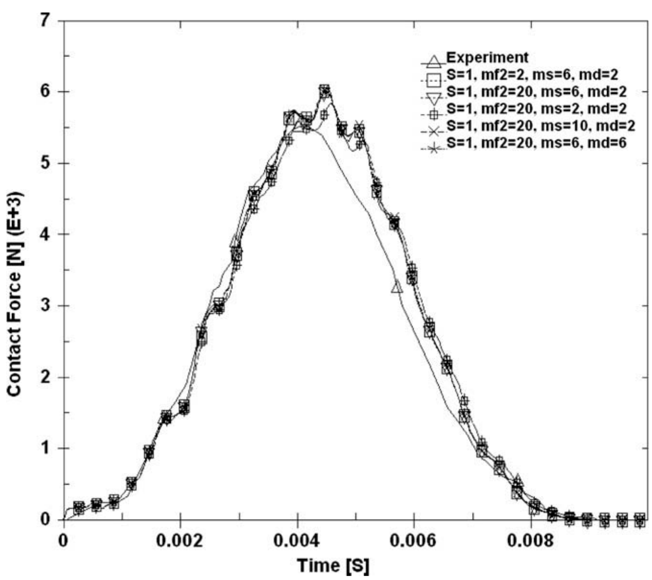

Fig. 10. Contact force–time history predicted by the current model using different values of damage parameters m_{f2}, m_s and m_d for a 27 *J* impact on a $[0_3/90_4/0_3]$ E-glass/Epoxy laminate.

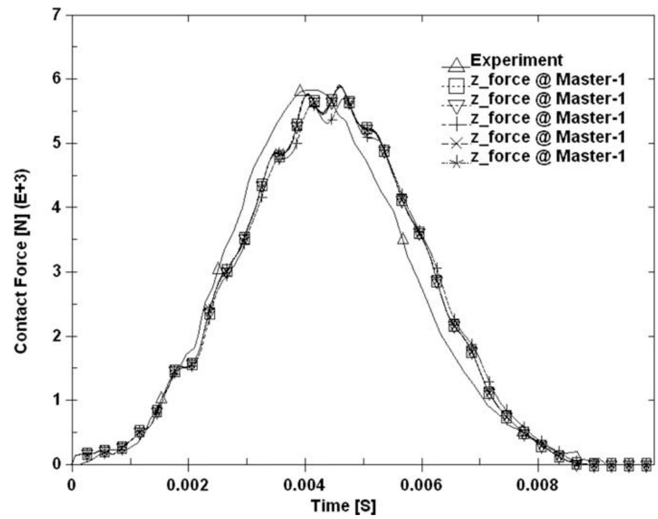

Fig. 11. Contact force–time history predicted by the current model using different values of damage parameters m_{f2}, m_s and m_d for a 27 *J* impact on a $[0_4/90_2/0_4]$ E-glass/Epoxy laminate.

behavior during unloading. Part of the reason for these inaccuracies can be attributed to the assumed properties for the constituents and the approximate boundary conditions. Overall, the predicted contact force history is found to agree reasonably well with the experimental result in each case.

Next, results of delamination area predicted by the current model in the three laminates are considered. In the experimental studies, the damaged specimens were visually inspected after impact for damage. Two butterfly wing-shaped delamination areas were observed at the interface between the 90° layer farthest from the impact point and the 0° layer below it, as shown in Figs. 18–20. It is to be noted here that delamination is not modeled explicitly in the current model but by using a CDM based approach. Therefore, it is predicted in the current simulations in the form of damaged elements at the center of the 90° layer farthest from the impact point whose through-the-thickness stress components are softened as discussed in the section on failure. Specifically, it is predicted in elements at the center of the third, fourth, and fifth layers from the bottom in the $[0_2/90_6/0_2]$, $[0_3/90_4/0_3]$, $[0_4/90_2/0_4]$ laminates, respectively.

Visual inspection of the damaged laminates in the experiments in [1] also revealed longitudinal matrix cracks going through the thickness of a layer in addition to delamination,. The first cracks visible to the naked eye were of a bending type in the unimpacted 0° layers due to rupture of the matrix and were followed by cracking in 90° layers and delamination, at the interface between two cracked layers. It was not possible to separate the appearance of the first cracks in 90° layers and delamination. The 90° layer cracks were shear cracks due to debonding of fiber/matrix interfaces. These observations point to two very significant characteristics of delamination: (1) it occurs when the layers on each side of the interface are locally cracked [1] and (2) the importance of a precise numerical representation of matrix cracking cannot be under-estimated [1].

Based on these observations and also the reason stated in the previous example, impact of the three different laminates is simulated for the following sets of damage parameters:

(a) *no shear damage*; $m_{f2} = 20$; $m_d = 2$.
(b) $m_s = 6$ ($\alpha_s = 1.3$); *no transverse damage*; $m_d = 2$.
(c) $m_s = 2$ ($\alpha_s = 2.25$); $m_{f2} = 20$; $m_d = 2$.
(d) $m_s = 6$ ($\alpha_s = 1.3$); $m_{f2} = 20$; $m_d = 2$.
(e) $m_s = 10$ ($\alpha_s = 1.2$); $m_{f2} = 20$; $m_d = 2$.

(f) $m_s = 6$ ($\alpha_s = 1.3$); $m_{f2} = 2$; $m_d = 2$.
(g) $m_s = 6$ ($\alpha_s = 1.3$); $m_{f2} = 10$; $m_d = 2$.
(h) $m_s = 6$ ($\alpha_s = 1.3$); $m_{f2} = 20$; $m_d = 4$.
(i) $m_s = 6$ ($\alpha_s = 1.3$); $m_{f2} = 20$; $m_d = 6$.

Scale factor S is taken to be equal to 1.0 in all these cases. Three different values of each of the damage parameters m_{f2}, m_s, and m_d are tested along with two special cases: (a) *no shear damage* and (b) *no transverse damage*. As discussed earlier, delamination is preceded by bending and shear type cracks in layers on either side of the interface. Hence, these special cases are chosen to analyze the role of transverse and shear damage functions in the current material model.

Evolution of the corresponding damage functions for the different values chosen are shown in Figs. 12–14. Damage values are plotted against strains for transverse, and shear modes and against the threshold function for delamination. In general, smaller exponents for constituent damage functions lead to an early initiation of damage and ductile behavior while higher values lead to a later initiation of damage and brittle behavior. Specific values of parameter α_s and m_s are chosen so that shear damage initiates at different strains and the damage function reaches almost zero at the ultimate failure strain of the matrix material. As seen in Fig. 13, shear damage evolution for $m_s = 2$ and $\alpha_s = 2.25$, starts early at a strain of about 0.5% and the shear moduli are reduced in a very ductile manner to close to zero at the ultimate shear strain value of 15%. At higher values of m_s and the corresponding α_s values, damage initiates at higher values and moduli reduction is less ductile. The delamination exponent does not control the initiation of delamination but only the post-failure degradation rate, which again increases with the exponent value, since the damage threshold has to reach a minimum value of 1 before the through-the-thickness stiffness are reduced. The delamination areas predicted in the various cases for the different laminates are shown in Figs. 15–17 and the results are discussed in the following sections. Incorrect results are predicted in some cases as discussed in the following sections and these are not shown in the figures.

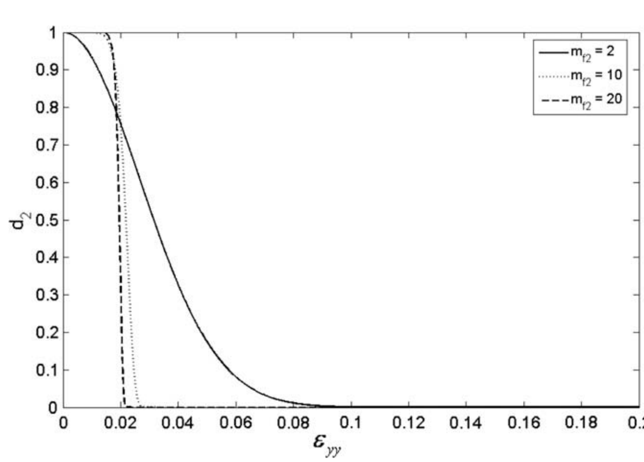

Fig. 12. Evolution of damage function d_2 with transverse normal strain.

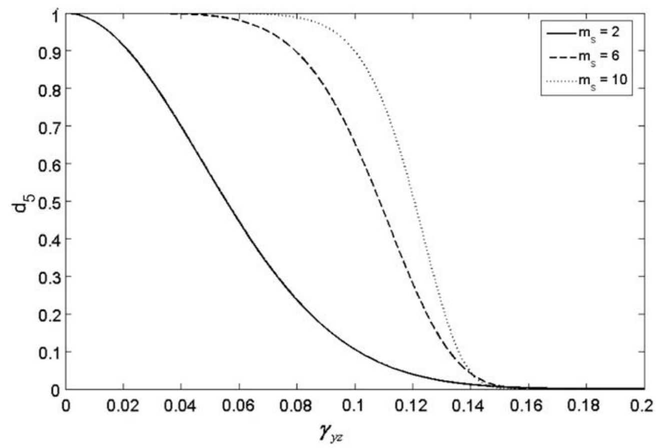

Fig. 13. Evolution of damage function d_5 with transverse shear strain.

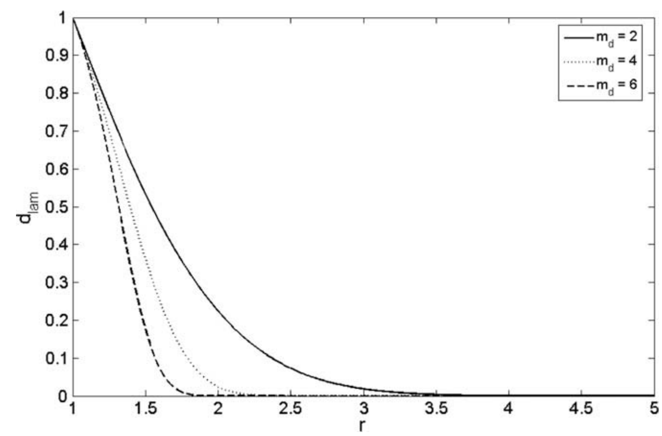

Fig. 14. Evolution of damage function d_{lam} with damage threshold (Eq. (42)).

7.3. Dependence of delamination area prediction on shear damage function – comparison of cases (a), (c), (d) and (e)

Without a separate damage function to account for matrix cracking (*no shear damage case*), the model still predicts delamination in all the laminates but it is predicted in the wrong layers. There is no specific pattern in the layers in which it is predicted but in general, it initiates in elements in which the through-the-thickness strains reach a combined value for which the damage threshold function is greater than 1 and then propagates to their neighboring elements. The fact that incorrect results are obtained in all the laminates for the "*no shear damage*" case clearly show that the delamination criterion used in the current model cannot predict delamination correctly if matrix cracking is not accounted for in the model.

With the shear damage function, delamination is predicted at the correct location for all the three values of m_s in the $[0_4/90_2/0_4]$ laminate while it is predicted in the

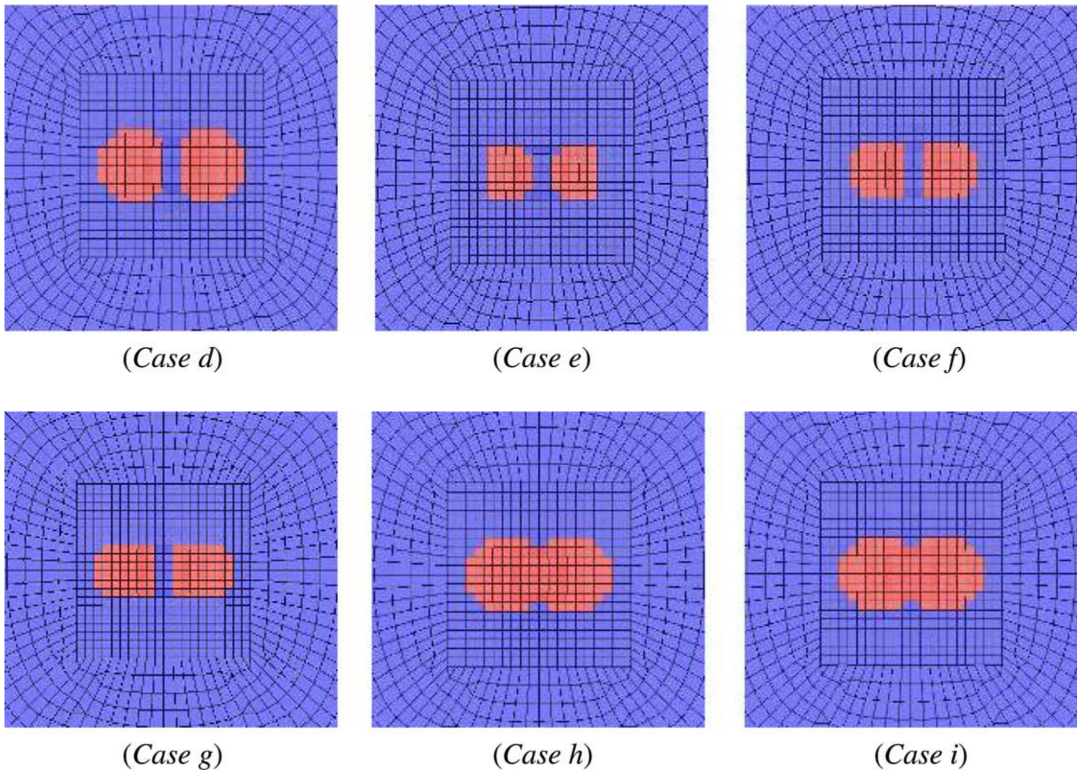

Fig. 15. Delamination areas predicted by the current model at the center of the third layer from bottom for a 27 *J* impact on a $[0_2/90_6/0_2]$ E-glass/Epoxy laminate.

wrong layers in the other two laminates for $m_s = 2$ ($\alpha_s = 2.25$), similar to the "*no shear damage*" case. In all laminates, the predicted delamination area decreases with increase in m_s indicating that the strain at which this damage mode is activated also plays a crucial role in the delamination prediction.

In general, these results indicate that a damage function that accurately captures the matrix cracking behavior of the composite, specifically the initiation and evolution of this damage mode, is crucial for accurate prediction of delamination using the criterion employed in the current model. Since the best results are obtained in the current model using $m_s = 6$ ($\alpha_s = 1.3$), this value is used in the simulations to study the variation of predicted delamination area with the other two damage parameters.

7.4. Dependence of delamination area prediction on transverse damage function – comparison of cases (b), (d), (f) and (g)

When the transverse failure mode is de-activated, the model predicts delamination in the correct layers for the $[0_3/90_4/0_3]$, and the $[0_4/90_2/0_4]$ laminates but not for the $[0_2/90_6/0_2]$. Also, the predicted delamination area increases considerably with increase in m_{f2} in the $[0_2/90_6/0_2]$ laminate while there is very minimal change in the other two laminates. These results show that the transverse damage function plays a significant role in the delamination prediction using the criterion employed in the current model in the $[0_2/90_6/0_2]$ laminate but not in the other two. The significant influence of the transverse damage function in the $[0_2/90_6/0_2]$ laminate can be attributed to the location of the delaminating interface. As the interface is moved farther from the mid-plane of the laminate, tensile strains in the layers on either side of the interface are considerably higher and the transverse shear strains are lower leading to this mode exerting more influence than the shear damage mode which is more influential as the interface is moved closer to the mid-plane. These results again show that the CDM based delamination criterion is not capable of predicting delamination correctly in all laminates and needs to be aided by other modes in a numerical model.

7.5. Dependence of delamination area prediction on through-the-thickness stiffness degradation exponent m_d – comparison of cases (d), (h) and (i)

As mentioned earlier, the exponent m_d controls only the rate of degradation after delamination is predicted in an element. In the $[0_2/90_6/0_2]$ and $[0_3/90_4/0_3]$ laminates, delamination is additionally predicted in elements between the two butterfly wing-shaped areas also for higher values of the exponent but there is no significant increase in the predicted area. In the $[0_4/90_2/0_4]$ laminate, there is no change observed in the predicted area. These results indicate that the delamination failure degradation exponent does not play any significant role in the prediction of delamination area using the current model.

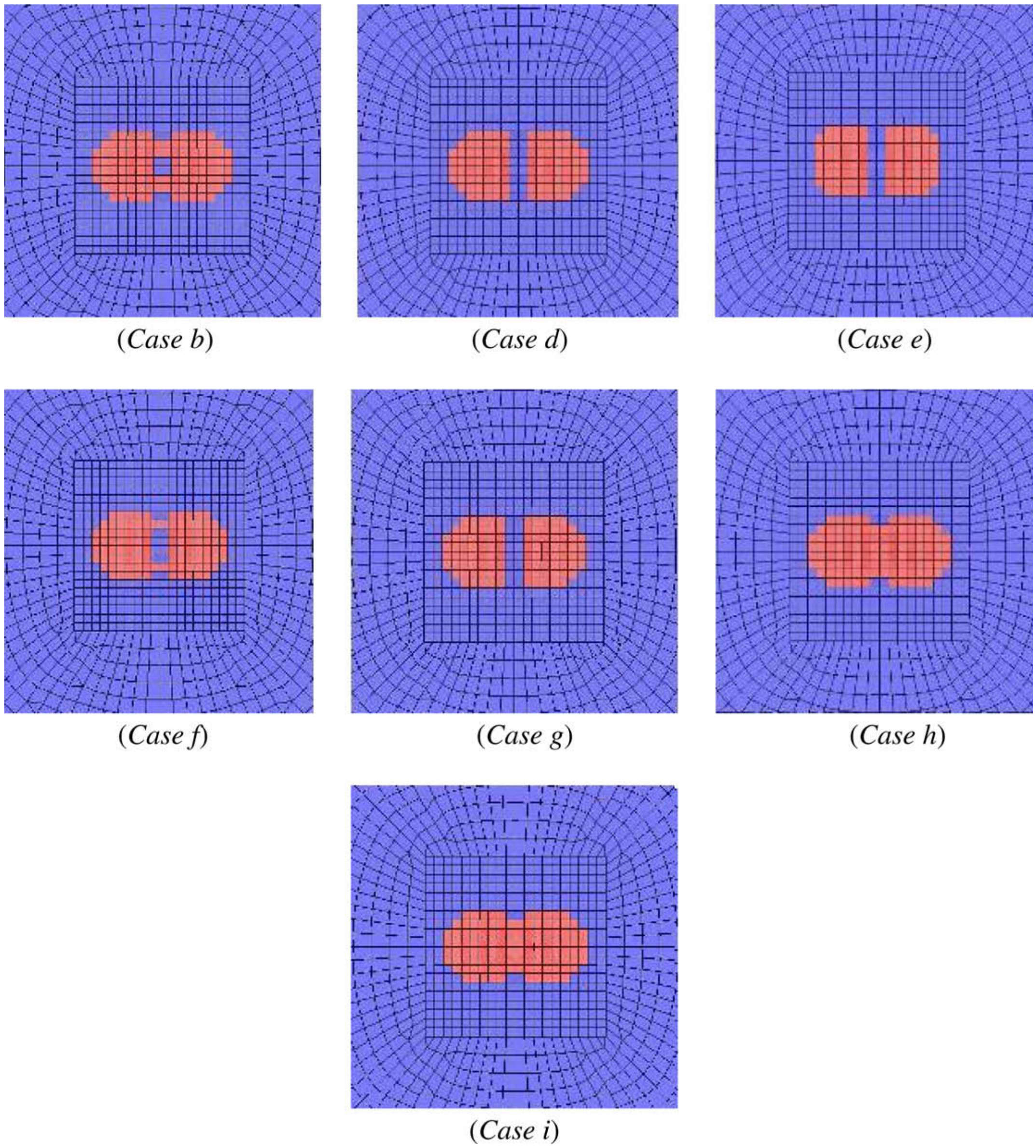

Fig. 16. Delamination areas predicted by the current model at the center of the fourth layer from bottom for a 27 J impact on a $[0_3/90_4/0_3]$ E-glass/Epoxy laminate.

7.6. Dependence of delamination area prediction on scale factor S

As mentioned earlier in the description of the delamination failure criterion, the scale factor S is originally introduced by Yen [18] to better correlate the predicted delamination area with experiments. Since the predicted delamination areas in the coarse mesh with $S = 1.0$ are almost as wide as the finer mesh region, a new FE model is created with a finer mesh in a larger region of the laminate close to the impact point and tested with the parameter values in *case (i)* given earlier and values of $S = 1.0$, 1.1, and 1.2. For $S = 1.0$, the delamination areas predicted using the finer mesh are found to be marginally more than the corresponding ones obtained earlier using the coarse mesh for all three laminates. For the other two values however, contrary to expectation, the results obtained are incorrect in all but one case with delamination being predicted in the wrong layers similar to the "no shear damage case" discussed earlier. Even in the one case in which location of the predicted area is correct, $S = 1.1$ for the $[0_3/90_4/0_3]$ laminate, there is no increase in the predicted area indicating that the scale factor does not play its intended role in the current model.

Finally, Figs. 18–20 show the maximum delamination areas predicted by the current model for the three laminates along with the experimental results. These results are obtained using the finer FE model with the parameter values in *case (i)* given earlier and $S = 1.0$. The predicted delamination areas are much lesser than the experimental results with the widths in particular being much lesser. Similar to the experimental results, however, the widths of the

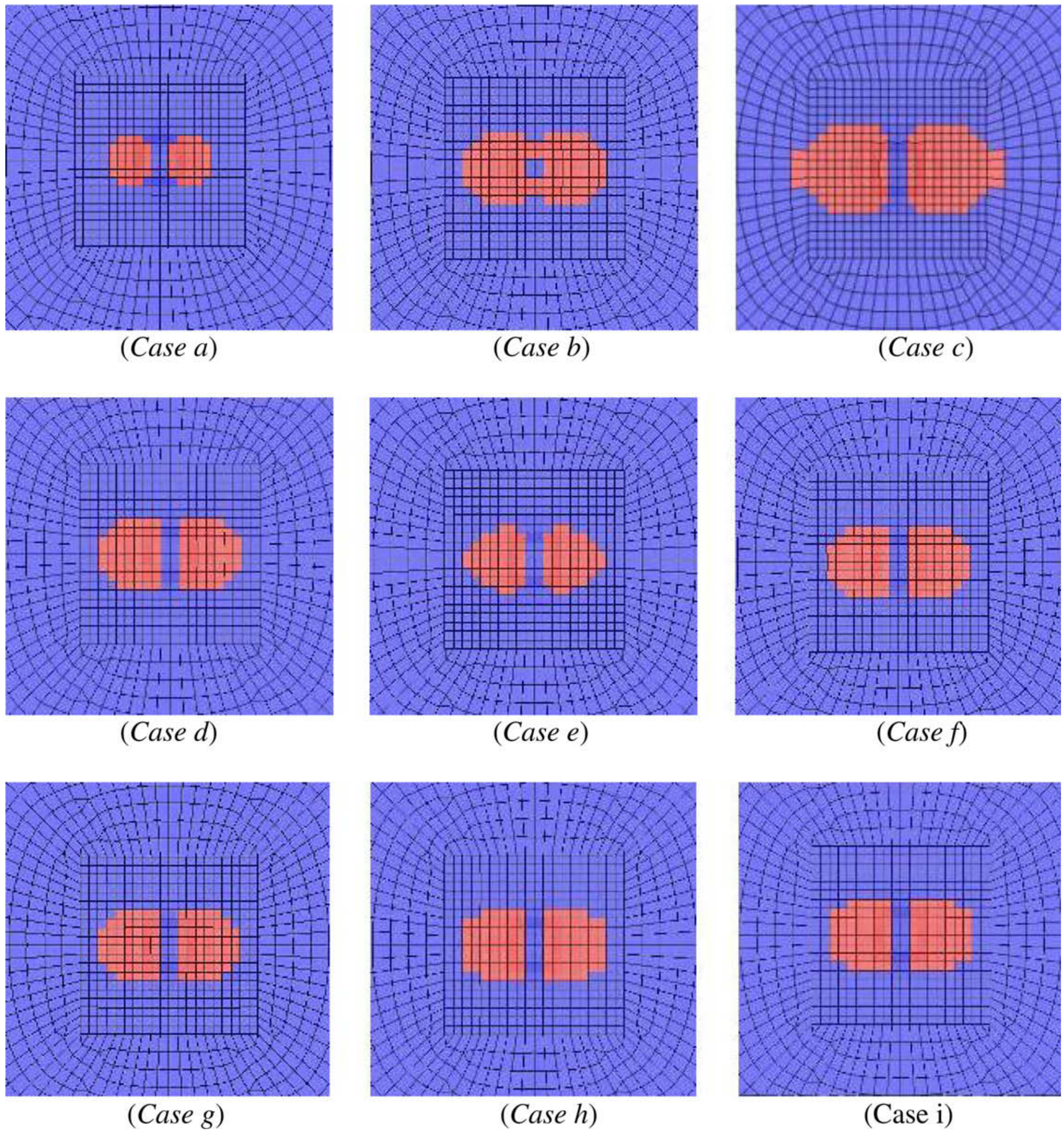

Fig. 17. Delamination areas predicted by the current model at the center of the fifth layer from bottom for a 27 J impact on a $[0_4/90_2/0_4]$ E-glass/Epoxy laminate.

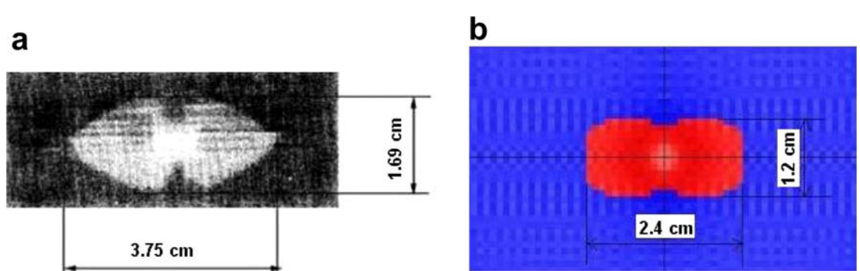

Fig. 18. Experimental and maximum predicted delamination areas at the center of the third layer from bottom for a 27 J impact on a $[0_2/90_6/0_2]$ E-glass/Epoxy laminate: (a) experiment (picture taken from Li et al. [6]); (b) current model with $S = 1.0$; $m_{f1} = 2$; $m_{f2} = 20$; $m_s = 6$; $m_d = 6$.

predicted delamination areas increase with increase in the number of 90° layer.

Delamination modeling approaches using a one-off stress-based failure criteria similar to the one used in the current model have also been used in similar efforts in the past, e.g. [1,18,23,24,26]. Although it was partially successful in some limited cases, its applicability to predict delamination damage remains unjustified [25] since the stress field is redistributed at the onset of delamination. Davies and Zhang [26] tried to employ the stress-based cri-

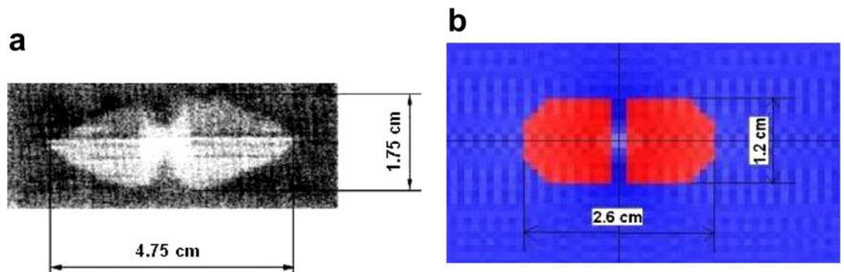

Fig. 19. Experimental and maximum predicted delamination areas at the center of the fourth layer from bottom for a 27 J impact on a $[0_3/90_4/0_3]$ E-glass/Epoxy laminate: (a) experiment (picture taken from Li et al. [6]); (b) current model with $S = 1.0$; $m_{f1} = 2$; $m_{f2} = 20$; $m_s = 6$; $m_d = 6$.

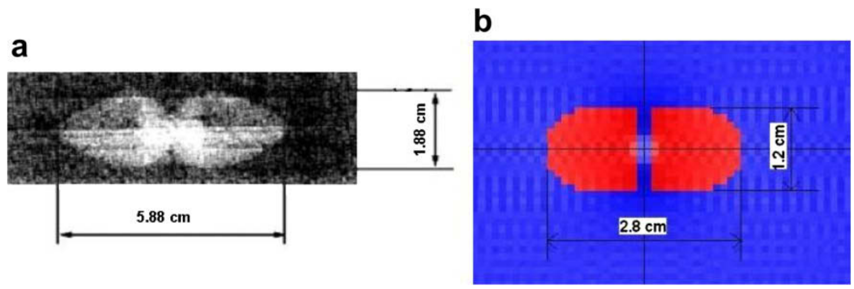

Fig. 20. Experimental and maximum predicted delamination areas at the center of the fifth layer from bottom for a 27 J impact on a $[0_4/90_2/0_4]$ E-glass/Epoxy laminate: (a) experiment (picture taken from Li et al. [6]); (b) current model with $S = 1.0$; $m_{f1} = 2$; $m_{f2} = 20$; $m_s = 6$; $m_d = 6$.

terion to predict the delamination sizes. Their conclusion is that it has clearly little relevance with reality except perhaps for the initial damage in the thinner plates, but only at the onset [5]. The results discussed here also lead to the same conclusion that the approach used in this model can at best be used as a preliminary test to check for initiation of delamination in laminates and determine potential sites and rough shapes but cannot give any realistic estimates of actual delamination area.

8. Summary and conclusions

A micro-mechanical model has been developed for unidirectional polymer matrix composites and implemented in the FE software LS-DYNA. It is well suited for impact loading conditions as it accounts for two important attributes of their mechanical behavior that is crucial for accuracy of such simulations namely strain-rate dependency and progressive post-failure behavior. Strain-rate dependency is incorporated by using viscoplastic constitutive relations based on a state variable approach for the resin constituent. Progressive post-failure behavior is modeled using a CDM based damage model. Different damage functions are used for various failure modes such as fiber failure, matrix cracking, and delamination and the response of the composite is softened according to the failure mode.

Though numerous micro-mechanical models have been developed in the past for modeling the behavior of unidirectional polymer matrix composites, there are very few that consider their progressive post-failure and even fewer that account for their strain-rate dependent behavior. Also, an extensive literature search did not reveal even a single one that accounts for delamination failure. The fact that the current micro-mechanical model has all these fore-mentioned features makes it a unique one. The model's predictions are validated by using it to simulate impact events for which experimental results are available in literature and comparing the predicted and experimental results. Contact force–time histories and fiber failure predicted by the model are found to agree very well with experimental results. However, delamination area is highly under-predicted indicating that the model can be used only as a preliminary test to check for delamination initiation and potential delamination sites.

Overall, the model is found to predict quite realistic results for impact simulations of unidirectional composite structures. However, as mentioned in Williams and Vaziri [7], there are a number of issues that need to be addressed in the CDM based damage model such as physical significance of the choice of damage parameters, and their dependence on mesh size and strain-rate to extend the effectiveness of this model. Also, a fracture mechanics approach may be more appropriate to model delamination.

References

[1] Collombet F, Lalbin X, Lataillade JL. Impact behavior of laminated composites: physical basis for finite element analysis. Compos Sci Technol 1998;58:463–78.
[2] Abrate S. Impact on laminated composite materials. Appl Mech Rev 1991;44(4):155–90.
[3] Abrate S. Impact on laminated composites: recent advances. Appl Mech Rev 1994;47(11):517–44.
[4] Cantwell WJ, Morton J. The impact resistance of composite materials – a review. Composites 1991;22(5):347–62.

[5] Li CF, Hu N, Yin YJ, Sekine H, Fukunaga H. Low-velocity impact-induced damage of continuous fiber-reinforced composite laminates. Part I. An FEM numerical model. Compos Part A: Appl Sci Manuf 2002;33:1055–62.
[6] Li CF, Hu N, Cheng JG, Fukunaga H, Sekine H. Low-velocity impact-induced damage of continuous fiber-reinforced composite laminates. Part II. Verification and numerical investigation. Compos Part A: Appl Sci Manuf 2002;33:1063–72.
[7] Williams KV, Vaziri R. Application of a damage mechanics model for predicting the impact response of composite materials. Comput Struct 2001;79:997–1011.
[8] Hallquist JO. LS-DYNA theory manual. Livermore: Livermore Software Technology Corporation (LSTC); 2006.
[9] Matzenmiller A, Lubliner J, Taylor RL. A constitutive model for anisotropic damage in fiber-composites. Mech Mater 1995;20(2):125–52.
[10] Van Hoof J, Woeswick MJ, Straznicky PV, Bolduc M, Tylko S. In: Proceedings of the fifth international LS-DYNA users conference; 1998.
[11] Goldberg R. Strain-rate dependent deformation and strength modeling of a polymer matrix composite utilizing a micro-mechanics approach. NASA/TM-1999-209768; 1999.
[12] Tabiei A, Yi W, Goldberg R. Non-linear strain-rate dependent micro-mechanical composite material model for finite element impact and crashworthiness simulation. Int J Non-Linear Mech 2005;40:957–70.
[13] Pecknold DA, Rahman S. Micromechanics based structural analysis of thick laminated composites. Comput Struct 1994;51(2):163–79.
[14] Tabiei A, Chen Q. Micromechanics based composite material model for crashworthiness explicit finite element simulation. J Thermoplast Compos Mater 2001;14:264–89.
[15] Tabiei A, Ivanov I. Micro-mechanical model with strain-rate dependency and damage for impact simulation of woven fabric composites. Mech Adv Mater Struct 2007;14(5):365–77.
[16] Goldberg RK, Stouffer DC. Strain rate dependent analysis of a polymer matrix composite utilizing a micromechanical approach. J Compos Mater 2002;36(7):773–93.
[17] Aminjikarai SB, Tabiei A. A strain-rate dependent 3-D micromechanical model for finite element simulations of plain weave composite structures. Compos Struct 2007;81(3):407–18.
[18] Yen CF. Ballistic impact modeling of composite materials. In: Proceedings of seventh international LS-DYNA users conference, Dearborn, Michigan; 2002. p. 6.15–.26.
[19] Delfosse D, Poursartip A. Experimental parameter study of static and dynamic out-of-plane loading of CFRP laminates. In: Poursartip A, Street KN, editors. Proceedings of the tenth international conference on composite materials (ICCM/10). Whistler: Woodhead Publishing; 1995. p. 583–90.
[20] Delfosse D, Poursartip A. Energy-based approach to impact damage in CFRP laminates. Composites 1997;28A:647–55.
[21] Delfosse D, Poursartip A, Coxon BR, Dost EF. Non-penetrating impact behavior of CFRP at low and intermediate velocities. In: Martin RH, editor. Composite materials: fatigue and fracture, ASTM STP 1230. Philadelphia: ASTM; 1995. p. 333–50.
[22] Xiao JR, Gamma BA, Gillespie Jr JW. Progressive damage and delamination in plain weave S-2 glass/SC-15 composites under quasi-static punch-shear loading. Compos Struct 2007;78(2):182–96.
[23] Choi HY, Chang FK. A model for predicting damage in graphite/epoxy laminated composites resulting from low-velocity impact. J Compos Mater 1992;26:2134–69.
[24] Hou JP, Petrinic N, Ruiz C, Hallett SR. Prediction of impact damage in composite plates. Compos Sci Technol 2000;60:273–81.
[25] Wang H, Vu-Khanh T. Fracture mechanics and mechanisms of impact-induced delamination in laminated composites. J Compos Mater 1995;29:156–78.
[26] Davies GAO, Zhang X. Impact damage prediction in carbon composite structures. Int J Impact Eng 1995;16:149–70.